Available online at www.sciencedirect.com
ScienceDirect
Journal of Solid State Chemistry 180 (2007) 496–509
JOURNAL OF SOLID STATE CHEMISTRY
www.elsevier.com/locate/jssc

# The $Pr_2Se_3$–$PrSe_2$ system: Studies of the phase relationships and the modulated crystal structure of $PrSe_{1.85}$

Thomas Doert[a,*], Christian Graf[a], Peer Schmidt[a], Inga G. Vasilieva[b], Paul Simon[c], Wilder Carrillo-Cabrera[c]

[a]*Inorganic Chemistry, Dresden University of Technology, Helmholtzstr. 10, 01069 Dresden, Germany*
[b]*A. V. Nikolaev Institute of Inorganic Chemistry, Russian Academy of Sciences, Siberian Branch, Acad. Lavrentiev Ave. 3, Novosibirsk, 630090, Russia*
[c]*Max Planck Institute for Chemical Physics of Solids, Nöthnitzer Str. 40, 01187 Dresden, Germany*

Received 14 September 2006; received in revised form 23 October 2006; accepted 26 October 2006
Available online 11 November 2006

**Abstract**

Thermochemical investigations have been carried out to elucidate the phase relationships in the system $Pr_2Se_3$–$PrSe_2$ and to construct the $p_{Se}$–$T$–$x$ diagram. The result of the tensimetric and thermogravimetric studies showed the thermal decomposition of $PrSe_2$ to be a step-wise process due to the formation of a sequence of discrete intermediate phases with the compositions $PrSe_{1.9}$, $PrSe_{1.85}$, $PrSe_{1.8}$, and $Pr_2Se_3$. $PrSe_{1.85}$ and $PrSe_{1.8}$ have been previously considered as selenium-deficient non-stoichiometric phases. Conclusions derived from the thermodynamic study were verified by X-ray diffraction and electron microscopy studies on single crystals of $PrSe_{1.85}$ which were obtained from reactions of praseodymium and selenium in stoichiometric amounts in a KCl flux at 1070 K. A two-dimensional modulation could be observed for $PrSe_{1.85}$ in X-ray and high-resolution transmission electron microscopy. The structure of $PrSe_{1.85}$ was solved and refined in superspace group $P4/n(\alpha\beta\frac{1}{2})(\beta-\alpha\frac{1}{2})00$ with lattice parameters of $a = 4.137(1)$ Å, $c = 8.398(2)$ Å of the basic unit cell and $\alpha = \beta = 0.293(1)$. The origin of the modulation can be attributed to a site occupancy wave and a charge density wave in its planar selenium layer. The experimentally determined magnetic moments indicate $Pr^{3+}$ for the polyselenides $PrSe_2$, $PrSe_{1.9}$ and $PrSe_{1.85}$.


*Keywords:* Tensimetric studies; Thermodynamic investigations; Polyselenides; Praseodymium; Modulated structure; HRTEM; $PrSe_{1.85}$

## 1. Introduction

The binary phase diagrams of rare earth metals, *Ln* (*Ln* = Y, La, Ce–Lu) and selenium which can be found in standard data bases and original communications are often incomplete and of poor reliability; the majority of systems is not even at hand (cf. [1], e.g., and references cited therein). However, the system Pr–Se has been investigated and three polyselenide phases, namely $PrSe_{2.33}$, $PrSe_{1.9}$ and $PrSe_{1.75}$ are stated here [1a]. $PrSe_{1.9}$ adopts the $CeSe_{1.9}$ structure type (space group $P4_2/n$) with lattice parameters $a = 9.296(2)$ and $c = 16.860(4)$ Å [2]. The existence of $PrSe_{2.33}$ ($Pr_3Se_7$) and $PrSe_{1.75}$ ($Pr_4Se_7$) is questionable, no structural data is available. Hints on polyselenide phases $PrSe_n$ with $1.5<n<1.9$ were nevertheless found during studies of the Pr–Se system (cf. [3], e.g.). These phases were mainly considered as non-stoichiometric derivatives of praseodymium diselenide $PrSe_2$. The crystal structure of stoichiometric $PrSe_2$ was refined from a twinned crystal recently. It crystallizes in space group $P2_1/a$ with lattice parameters $a = 8.396(2)$ Å, $b = 4.184(1)$ Å, $c = 8.431(2)$ Å, and $\beta = 90.08(4)^\circ$ [4] and adopts a twofold superstructure of a ZrSSi-type basic structure due to the formation of $Se_2^{2-}$ dimers in the planar selenium layers of the structure.

In this work, we performed thermodynamic studies on praseodymium polyselenides $PrSe_n$ ($1.5<n<2$) to determine the compositions of the polyselenide phases and their phase relationships. High-resolution transmission electron microscopy and X-ray investigations were carried out to elucidate the structure of the hitherto unknown modulated phase $PrSe_{1.85}$.

*Corresponding author. Fax: +49 351 463 37287.
*E-mail address:* thomas.doert@chemie.tu-dresden.de (T. Doert).

0022-4596/$ - see front matter © 2006 Published by Elsevier Inc.
doi:10.1016/j.jssc.2006.10.030

## 2. Experimental

### 2.1. Sample preparation

Crystals of $PrSe_2$ as samples for thermogravimetric and tensimetric studies were prepared by different synthetic routes. The preparation by chemical vapor transport reaction using iodine as transport agent has been described previously [4]; phase pure crystalline samples of $PrSe_2$ can be obtained following this route. An alternative route is the preparation by metathesis according to the reaction:

$$2\ PrCl_3 + 3\ K_2Se_2 \rightarrow 6\ KCl + 2\ PrSe_2 + 2\ Se.$$

Anhydrous $PrCl_3$ (powder, 99.9%) was used as obtained (Strem Chemicals, Kehl, Germany); $K_2Se_2$ has been prepared by reaction of stoichiometric amounts of potassium (ingot, 99.99 %, Chempur, Karlsruhe, Germany) with selenium (powder, 99.99 %, Strem) in liquid ammonia at 210 K. The reaction mixtures were filled in silica ampoules in an argon-filled glove box. The ampoules were flame-sealed under dynamic vacuum, placed in a furnace, heated for 8 days at 1070 K and cooled with 3 K/h to room temperature. The excess selenium formed during the reaction could be removed by sublimation. For that, the bottom of the ampoules containing the reaction products were inserted in a vertical tubular furnace; the furnace temperature was held at 720 K for 20 h, e.g. The duration of the sublimation procedure was varied between 4 and 30 h according to the desired excess of free Se for the tensimetric studies. Se deposits at the tops of the ampoules, which were kept at room temperature outside the furnace. As can be seen from the thermogravimetric study (Fig. 1), decomposition of $PrSe_2$ doesn't occur at temperatures below 800 K. After opening the ampoules, KCl which intermediately acted as internal flux material for the crystallization of the diselenide can be removed by rinsing the reaction product with a mixture of ethanol and water. Well-crystallized samples of praseodymium diselenide and, if desired, additional selenium were obtained. X-ray powder diagrams proved the samples to consist of $PrSe_2$ or $PrSe_2$ and selenium only. EDX measurements (Zeiss scanning electron microscope 982 Gemini with Noram Voyager analytic unit) on selected crystals of $PrSe_2$ showed no impurities.

Single crystals of $PrSe_{1.85}$ have been prepared by reaction of stoichiometric amounts of the elements (Pr: rod, 99.9%, Strem; Se: s. above) in a KCl flux (KCl powder, 99.9 %, Fluka, Bwchs, Switzerland; pre-heated under dynamic vacuum prior to use). The reactions were performed in silica ampoules which were filled under argon, flame-sealed under dynamic vacuum, placed in a furnace, heated for 8 days at 1070 K and cooled with a ratio of 3 K/h to room temperature. After cooling, the KCl flux was removed with a mixture of ethanol and water and silvery-grey, air stable platelets of $PrSe_{1.85}$ were obtained. EDX measurements on several crystals of $PrSe_{1.85}$ revealed no impurities.

### 2.2. Thermochemical investigations

Thermogravimetric measurements were performed with heating ratios of 5 K/min under argon (99.999 %, Messer-Griesheim, Krefeld, Germany) using a Netzsch DTA/TG 449C to determine the mass loss starting from crystalline samples of $PrSe_2$.

Tensimetric studies were performed in a self-made manometer using the static membrane technique. Details

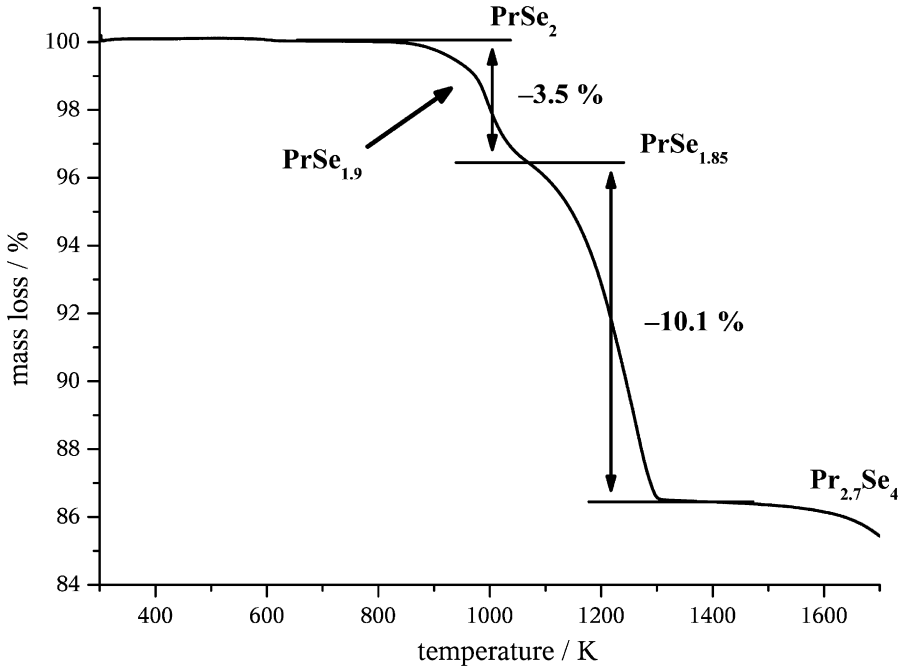


Fig. 1. Mass loss/% of a sample of $PrSe_2$ between 300 and 1700 K.

on the apparatus and investigation procedure can be found in e.g., [5]. Two series of homogeneous samples consisting of crystals of pure $PrSe_{2.00\pm0.01}$ (the composition results from X-ray structure analyses of several crystals) as well as $PrSe_{2.00\pm0.01}$ containing a small amount of free selenium were the subjects of the study. A certain amount of the initial sample was placed in a closed pre-evacuated vessel with the volume ($V$; $V \gg V_c$ where $V_c$ is the volume of the condensed phase) to measure the total vapor pressure $p_{total}$ upon heating. In a closed system, the initial composition of the condensed phase ($PrSe_2$ or $PrSe_2+n$ Se) shifts gradually towards the composition $Pr_2Se_3$ because of the preferential transition of selenium into the vapor phase. The process can be understood as an incongruent decomposition into the gas phase. As the total vapor pressure is dominated by gaseous $Se_2$, the step-like decomposition of the condensed phase can be used to calculate the composition of the intermediate praseodymium selenides. $Pr_2Se_3$ does not decompose up to $T = 1500$ K and can thus be regarded as the metal-rich border composition for our studies. To cover the whole composition range between $PrSe_2$ and $Pr_2Se_3$ different amounts of the initial samples were used.

### 2.3. Magnetic measurements

Temperature-dependent magnetic susceptibilities of the compounds $PrSe_2$, $PrSe_{1.9}$ and $PrSe_{1.85}$ were determined on *squid* magnetometer (*MPMS,* Quantum Design) in a magnetic field of 1 T between 2 and 400 K.

### 2.4. Electron microscopy

HRTEM investigations were carried out at the Triebenberg Special Laboratory (Dresden) with a Philips CM200 FEG/Super Twin-Lorentz Microscope. The microscope was equipped with a field emission gun operating with an accelerating voltage of 200 kV. Micrographs were recorded with a $1 \times 1$ k CCD-camera and fed into the computer for on-line processing and reconstruction in nearly real-time mode. The images were evaluated using the software Digital Micrograph 3.3.1 (Gatan). For these investigations, the crystals from flux reactions were ground under ethanol. Some drops of this suspension were placed on a copper grid coated with a perforated carbon foil. The ethanol was then allowed to evaporate. Due to their laminar structure, the crystals cleave quite easily to give very thin platelets, some being transparent to the electron beam. No precautions against radiation damages were taken.

### 2.5. Single crystal X-ray investigations

Buerger precession photographs were recorded to check the quality of several crystals of $PrSe_{1.85}$, to determine the lattice parameters and to confirm the presence of satellite reflections. One crystal of appropriate quality was subsequently placed on a diffractometer (STOE IPDS-II, Mo$K\alpha$ radiation, graphite monochromator) and complete data sets were recorded at 293 and 120 K. Integration of the data, as well as Lorentz and polarization factor corrections haven been performed with the IPDS software package [6]; the modulation vectors $q_1$ and $q_2$ have been determined and refined with the IPDS software package, too. A numerical absorption correction was applied based on the experimentally determined crystal shape using the program JANA2000 [7]. Full-matrix least-squares refinements were carried out with JANA2000 against $F^2$; extinction effects were corrected according to Becker and Coppens [8]. Both X-ray data sets reveal no discrepancies: The modulation vectors remain unchanged in the investigated temperature interval, the intensities of the satellites increases slightly at lower temperatures. Thus, only the results of the low-temperature data are discussed and presented in the following.

## 3. Results and discussion

### 3.1. Thermogravimetry

The mass loss as a function of temperature (TG plot) is displayed in Fig. 1. Starting from $PrSe_2$, two steps in the decomposition curve can be made out. One corresponds to the intermediate formation of a sample of the composition $PrSe_{1.85}$, the second one to the formation of a compound with the composition $PrSe_{1.48}$. The latter phase was identified as $C$-type $Pr_2Se_3$ by its X-ray powder diagram after cooling of the sample. $C$-$Pr_2Se_3$, like several other rare earth sesquichalcogenides, crystallizes in a cation defect variant of the $Th_3P_4$ structure in space group $I\bar{4}3d$, [9]. There is at least one further kink (indicated by an arrow in Fig. 1) in the TG plot which can be attributed to the intermediate formation of $PrSe_{1.9}$.

### 3.2. Tensimetric measurements

Fig. 2 shows the $\lg p_{total}$–$1/T$ curves of seven experiments starting from $PrSe_2$ or ($PrSe_2$ + Se) samples and one experiment starting from elemental selenium for reasons of comparison. The vapor pressure in the experiments starting from pure $PrSe_2$ increases due to the formation of polyselenide phases $PrSe_n$ with $n<2$ while excess Se evaporates:

$$PrSe_2(s) \rightarrow PrSe_{2-x}(s) + x/2\ Se_2(g)$$

(s in parentheses stands for solid and g for gasous in the following). In the second case, i.e., starting from a mixture of $PrSe_2$ + Se, the vapor pressure is initially determined by the partial pressure of Se as can be seen by comparison with the $\lg p$–$1/T$ plot of elemental Se. This means, that no polyselenides of praseodymium $PrSe_n$ with $n>2$—like e.g., $PrSe_{2.33}$,—are formed under the conditions of the metathesis reaction.

The shapes of the $\lg p_{total}$–$1/T$ functions (the number of steps) are determined by the ratio $m/V$, where $m$ is the mass

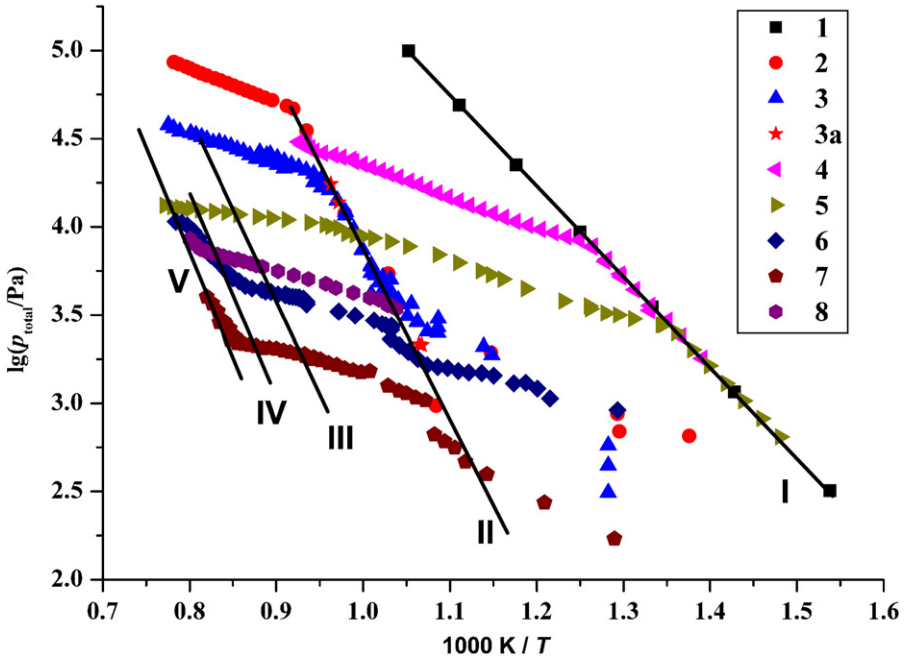


Fig. 2. $\lg p_{total}$–$1/T$ dependences of evaporation of $PrSe_2$ and ($PrSe_2$ + Se) with the $m/V$ values of experiments 2–8 from Table 1; experiment 1 shows the evaporation of pure Se for comparison.

of the initial condensed phase ($PrSe_2$ or $PrSe_2$ + Se, respectively) and $V$ the vessel volume, Table 1. The step-like forms for all functions reflect the changes in the condensed phase at definite temperatures due to changes of the initial three-phase equilibrium (solid 1/solid 2/gas phase) to a two-phase equilibrium (solid 2/gas phase) and vice versa (solid 2/solid 3/gas phase). The gas phase can be regarded as consisting of pure $Se_2$ (g), cf. discussion of Fig. 5 below. Pairs of corresponding adjacent intermediate polyselenide phases and finally $Pr_2Se_3$ are in equilibrium with the vapor phase. The lines have various junctions depending on the $m/V$ values. Junctions on the monovariant lines determine the complete disappearance of the selenium richer phase while almost horizontal lines ($p = nRT/V$) located between each pair of the three-phase lines reflect the equilibrium between corresponding intermediates with the vapor in a definite temperature range.

The results of each experiment were used to calculate the composition of the intermediate polyselenide phases corresponding to a definite total pressure at a given temperature. The positions of all junctions can be extracted from Fig. 2, except for the part of the curves placed between the lines II and III. The uncertainty of the determination of the compositions can be reduced, if the molar Se/Pr ratio values of the condensed phase are calculated for the whole $\lg p_{total}$–$1/T$ lines and plotted as a function of temperature. The composition calculation was made using the ideal gas equation:

$$\left(\frac{N_{Se}}{N_{Pr}}\right) = \left(\frac{N^0 - p_{Se(2),ij} RT_{ij} \Big/ n_{ij} V_j}{m_j M}\right),$$

where $(N_{Se}/N_{Pr})_{i,j}$ is the atomic ratio in the condensed phase at a temperature $T_{ij}$ for any data point $i$ of experiment $j$, $N^0$ is the initial amount of Se in the sample, $p_{Se(2)ij}$ is the partial pressure of $Se_2$ calculated from the experimental total pressure based on values of the equilibrium constants for the reaction $Se_n = n/2\ Se_2$ [10], $n_{ij}$ is the number of moles of $Se_2$ in the gas phase, $V_j$ is the volume of the membrane vessel, $m_j$ is the initial sample mass and $M$ is the molecular mass of $PrSe_2$. If the accuracies of the experiments are in the following range: about 1 K for temperature measurements, about 13 Pa for the vapor pressure, about 0.1 mL for the vessel volume, and about $10^{-5}$ g for the sample mass, it is possible to determine the intermediate compositions with a precision of about 0.2 at% as has been shown in [5]. The final compositions calculated are presented in Table 1 (last column) and shown graphically for some experiments for different intermediate levels of selenium content in Fig. 3a–c. To extract further details of the compositions of the polyselenides, isotherms of the $Se_2$ partial pressure against the Se/Pr ratio were plotted. The general appearance of such isotherms are very much alike, the isotherm for $T = 1163$ K is given in Fig. 3d.

In Fig. 4, the phase barogram of the system $Pr_2Se_3$–$PrSe_2$ is presented where the three-phase lines $PrSe_2$ (s)/$PrSe_{1.9}$ (s)/$Se_2$ (g) (II), $PrSe_{1.9}$ (s)/$PrSe_{1.85}$ (s)/$Se_2$ (g) (III), $PrSe_{1.85}$ (s)/$PrSe_{1.8}$ (s)/$Se_2$ (g) (IV) and $PrSe_{1.8}$ (s)/$PrSe_{1.5}$ (s)/$Se_2$ (g) (V) are constructed based on the $(N_{Se}/N_{Pr})_i$ vs. $1/T$ functions.

From this diagram the coefficients $A$ and $B$ of the pressure function

$$\lg(p(Se_2)/\text{Torr}) = A - B/T$$

Table 1
Conditions and results of the tensimetric experiments

| Exp. no. | $M$(g) | $V$(cm$^3$) | $T$(K) | $p$ (total)/(Torr) | $m \cdot 1000$(V) | Se/Pr ratio | |
|---|---|---|---|---|---|---|---|
| | | | | | | Start | final |
| 1 | Free Se [10] | | | | | | |
| 2 | 0.1748 | 4.5 | 726–1279 | 7–644 | 38.8 | 2.00 | 1.916 |
| 3 | 0.1270 | 10.11 | 780–1280 | 3–285 | 12.6 | 2.016 | 1.845 |
| 4 | 0.0451 | 22.37 | 719–1080 | 16–230 | 2.02 | 3.237 | 1.805 |
| 5 | 0.0550 | 72.85 | 675–1296 | 5–99 | 0.75 | 3.200 | 1.921 |
| 6 | 0.0573 | 59.38 | 773–1275 | 7–80 | 0.96 | 2.153 | 1.500 |
| 7 | 0.0332 | 59.38 | 775–1220 | 1–35 | 0.56 | 2.060 | 1.561 |
| 8 | 0.0410 | 17.80 | 960–1250 | 26–64 | 2.3 | 2.00 | 1.814 |

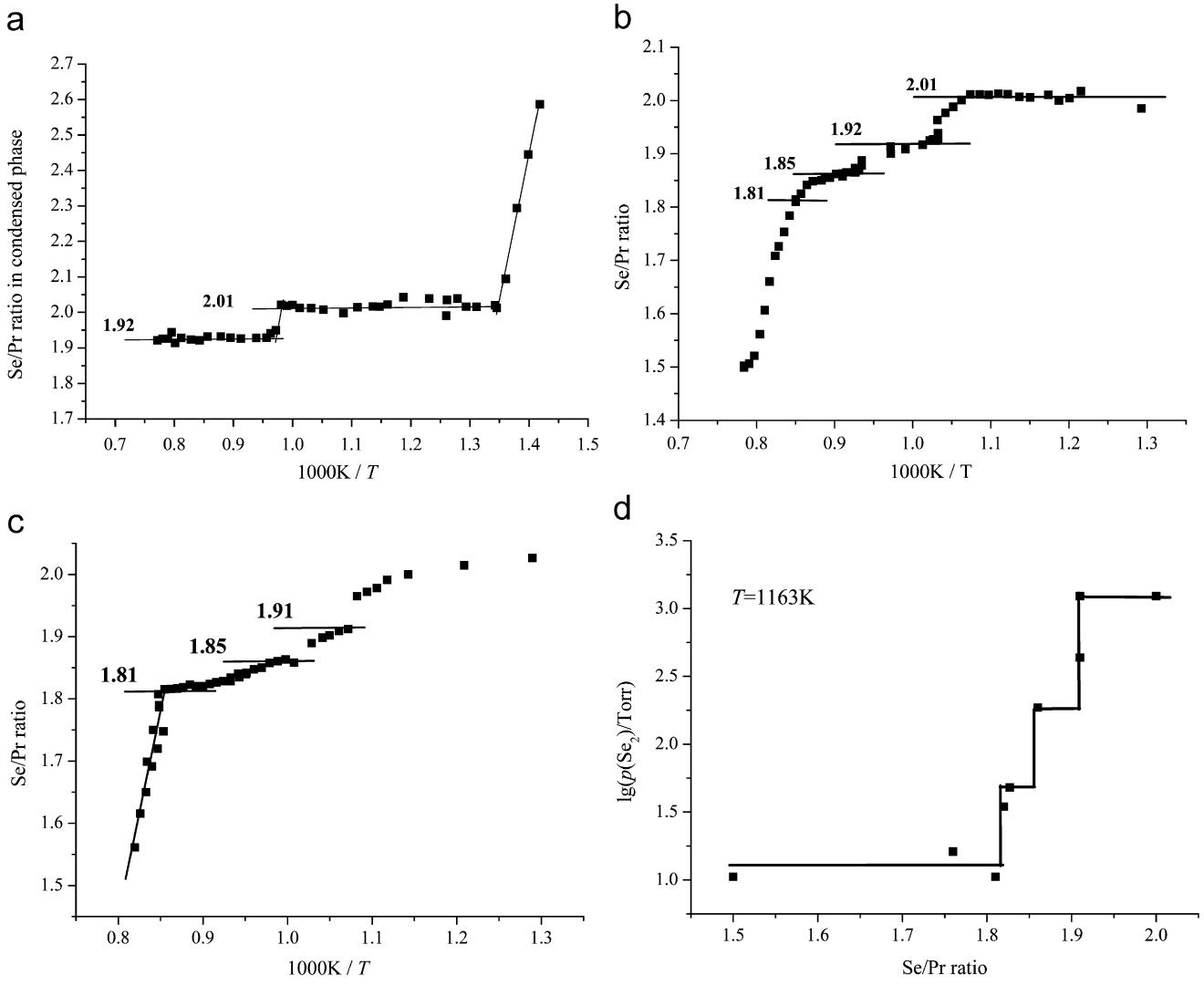


Fig. 3. Variation of Se/Pr value in the condensed phases with temperature for experiment 5 (a); 6 (b); and 7 (c), compositions of intermediate phases are indicated; (d) one of the $Se_2$ partial pressure isotherms within the compositional range $PrSe_{1.5}$–$PrSe_2$ at $T = 1163$ K.

were calculated (Table 2). Following the equation

$$lg\, p = A - \frac{B}{T} = \frac{\Delta S^{\circ}_R(T)}{R} - \frac{\Delta H^{\circ}_R(T)}{R}\frac{1}{T}$$

the standard enthalpies and entropies for the decomposition reactions were calculated. The standard enthalpies and entropies of formation of the praseodymium polyselenides were then obtained using the thermal decomposition functions, the *Neumann-Kopp* rule and standard data given in [20,21]; the results are stated in Table 3. The thermodynamic modelling [11] of the solid–gas equilibria using the standard data finally shows the consistency of the data with

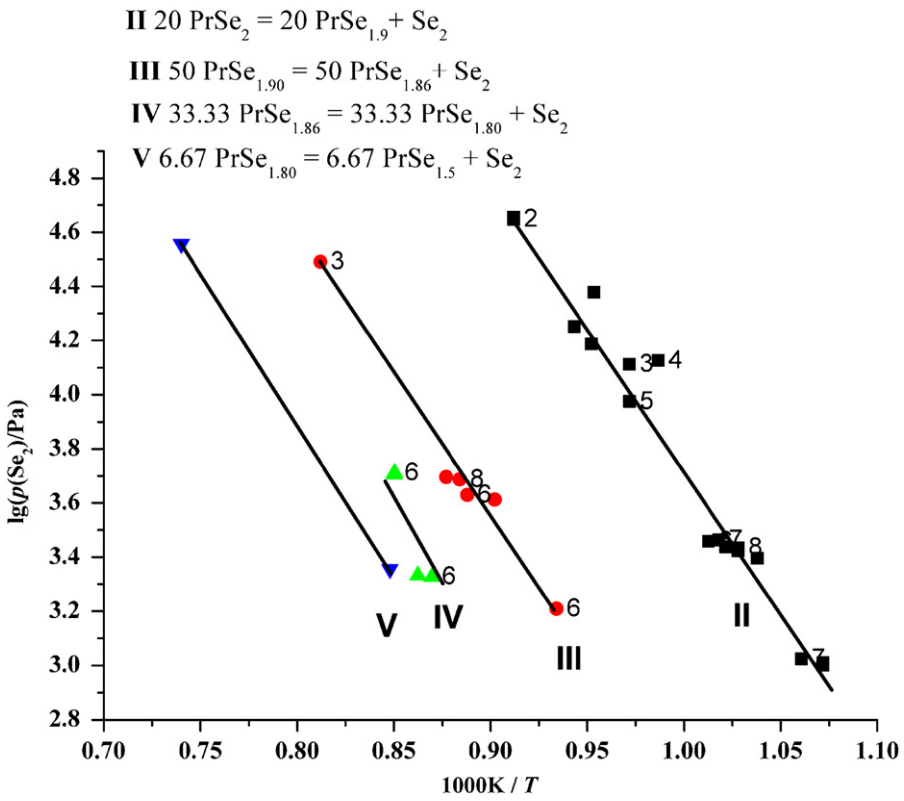


Fig. 4. The three-phase equilibrium lines (II–V) of the $p$–$T$ projection of the $Pr_2Se_3$–$PrSe_2$ phase diagram according to results of experiments 2–8.

Table 2
Coefficients of the pressure function ($\lg(p(Se_2)/Torr) = A - B/T$) for the decomposition reaction of the Praseodymium polyselenides $PrSe_n$

| Decomposition reaction | $A$ | $B$ |
|---|---|---|
| 20 $PrSe_{2.00}$ (s) = 20 $PrSe_{1.90}$ (s) + $Se_2$ (g) | 11.4 ± 0.2 | 9800 ± 200 |
| 40 $PrSe_{1.90}$ (s) = 40 $PrSe_{1.85}$ (s) + $Se_2$ (g) | 12.1 ± 0.2 | 12000 ± 200 |
| 40 $PrSe_{1.85}$ (s) = 40 $PrSe_{1.80}$ (s) + $Se_2$ (g) | 12.5 ± 0.2 | 12900 ± 200 |
| 6.67 $PrSe_{1.80}$ (s) = 6.67 $PrSe_{1.50}$ (s) + $Se_2$ (g) | 12.1 ± 0.5 | 13000 ± 500 |

the observed thermal behavior. As predicted, $Se_2$ (g) is the dominating gas species with $p(Se_2) > 10^3\ p_i$ ($i = Se_x$; PrSe, Pr); Fig. 5.

According to the data plotted in Figs. 2, 3d and 4, the polyselenide phases $PrSe_2$, $PrSe_{1.90}$, $PrSe_{1.85}$, and $PrSe_{1.80}$ have no homogeneity regions within an experimental error of about 0.2 at% of Se, corresponding to standard deviations of about 0.01 for the stoichiometric coefficient $n$ in the formulae $PrSe_n$. All intermediate phases should be considered as stoichiometric phases. For $PrSe_2$ and $PrSe_{1.9}$, X-ray structure data are consistent with these results [2,4]. In order to check this conclusion for the compounds with lower selenium content, structural studies on $PrSe_{1.85}$ were carried out.

### 3.3. Magnetic data

The magnetic susceptibilities of the three polyselenides $PrSe_2$, $PrSe_{1.9}$ and $PrSe_{1.85}$ obey the Curie-Weiss law for $T > 100$ K. Negative Curie temperatures for $PrSe_2$ ($\theta = -27$ K) and $PrSe_{1.85}$ ($\theta = -21$ K) indicate antiferromagnetic ordering, a positive Curie temperature for $PrSe_{1.9}$ ($\theta = 20$ K) indicate ferromagnetic ordering for $T < 20$ K. The magnetic moments derived from these experiments at 300 K are 3.65 $\mu_B$ for $PrSe_2$, 3.6 $\mu_B$ for $PrSe_{1.9}$ and 3.64 $\mu_B$ for $PrSe_{1.85}$ in good agreement with the theoretical value of 3.62 $\mu_B$ [12] for trivalent praseodymium ($Pr^{3+}$).

### 3.4. Transmission electron microscopy

The TEM images of crystallites of $PrSe_{1.85}$ show homogenous domains which appear widely ordered. The domain size found over a variety of crystallites is in the range of several nanometers. Fig. 6 displays high-resolution TEM images along [1 1 0] (Figs. 6a and c) and along [0 1 0] (Figs. 6d and f). The modulation can be observed as periodic variations in contrast, e.g., along ~[$\bar{7}$ 7 4] (Fig. 6c) and [1 0 0] (Fig. 6f). The Fourier Transforms (FTs) of both

Table 3
Standard enthalpies und entropies of the Praseodymium polyselenides $PrSe_n$ calculated using the thermal decomposition functions

| Phase | $\Delta H^\circ(298)$(kJ mol$^{-1}$) | $S^\circ$(298) (J mol$^{-1}$ K$^{-1}$) | $\tilde{C}_p$(800)(J mol$^{-1}$ K$^{-1}$) | $S^\circ$(298) (J mol$^{-1}$ K$^{-1}$) Neumann–Kopp[a] |
|---|---|---|---|---|
| $Pr_{(s)}$ | 0 [20] | 73.9 [20] | 35.2 [20] | |
| $Se_{(s)}$ | 0 [20] | 42.3 [20] | 35.7 [20] | |
| $PrSe_{2(s)}$ | −527.1±4 | 132.4±4 | 81.0±0.5 | 132.6 |
| $PrSe_{1.90(s)}$ | −523.9±8 | 129.1±8 | 78.3±0.5 | 128.4±8 |
| $PrSe_{1.85(s)}$ | −521.4±12 | 127.8±12 | 77.2±0.5 | 126.7±8 |
| $PrSe_{1.80(s)}$ | −518.3±16 | 126.8±16 | 75.5±0.5 | 124.1±8 |
| $PrSe_{1.50(s)}$ | −499.8±40 | 118.0±40 | 67.5±0.5 | 111.5±8 |
| | −470.7 [21] | 119.3 [21] | | |
| $PrSe_{(s)}$ | −359.8±40 | 90.3 [21] | 55.0 | |

[a]Neumann–Kopp–rule: $\Delta S_R = 0$; $S^\circ(298, PrSe_{2-x}) = S^\circ(298, PrSe) + (1-x)\ S^\circ(298, Se)$.

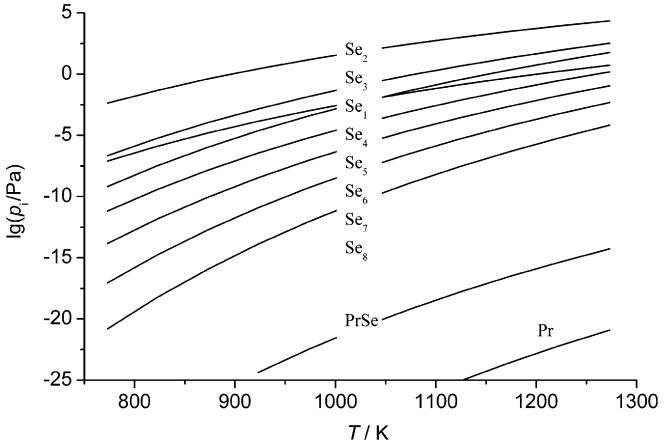


Fig. 5. Temperature dependence of the partial pressures of the gase phase species over a solid $PrSe_{1.8}/PrSe_{1.85}$; calculated with the thermodynamic standard data (Table 3) and the program TRAGMIN [11].

images (corresponding to the diffraction patterns) show, apart from the main reflections, satellites corresponding to the modulation vector $q_1$ (Fig. 6b; see black arrows) and satellites running along $a^*$ (Fig. 6e, see gray arrows) originated by the so-called cross-terms which are reflections corresponding to modulation vectors $\pm(q_1+q_2)$ and $\pm(q_1-q_2)$. Cross-terms are evidence for a two-dimensional modulation, they cannot be induced by twinning. The translational part of $\frac{1}{2}$ along $c^*$ of the modulation vector can clearly be seen in Fig. 6b.

### 3.5. X-ray structure determination

The data collection at $T = 120$ K revealed lattice parameters of $a = 4.137(1)$ Å and $c = 8.398(2)$ Å of the basic unit cell and modulation vectors $q_1 = (-0.293(1), 0.293(1), \frac{1}{2})$ and $q_2 = (0.293(1), 0.293(1), \frac{1}{2})$. Since cross-terms were observed in the FT's of the HRTEM images and in X-ray diffraction, only (3+2)-dimensional superspace group were considered for the refinement of the modulated structure. According to the reflection conditions, the tetragonal superspace groups $P4/nmm(\alpha\alpha\frac{1}{2})(\alpha-\alpha\frac{1}{2})00$ mm with $\alpha = 0.293(1)$ (no. 3076 according to [13]) and $P4/n(\alpha\beta\frac{1}{2})(\beta-\alpha\frac{1}{2})00$ with $\alpha = \beta = 0.293(1)$ (no. 2593; [13]) were taken into account. In order to lose the commensurate part of the modulation vectors, the $c$-axis of the unit cell of the average structure was doubled and the superspace centering condition (0,0, 1/2,1/2,1/2) was introduced; the modulation vectors then take the form $q'_1 = (-0.293(1), 0.293(1), 0)$ and $q'_2 = (0.293(1), 0.293(1), 0)$ (cf. Table 4). The modulated structure was refined in both using the transformed atomic coordinates of the basic ZrSSi type structure as starting positions. According to the crystallographic agreement factors, the distribution of interatomic distances and the standard deviations the best fit was achieved in superspace group $P4/n(\alpha\beta\frac{1}{2})(\beta-\alpha\frac{1}{2})00$ considering twinning according to (0 1 0, 1 0 0, 0 0 1); the respective structure is described in the following.

The conventional three dimensional refinement of the average structure converged to $wR_2 = 0.114$ for all 223 independent main reflections. Se(2), the selenium atom of the square layer, showed large anisotropic displacement parameters along $a$ and $b$, indicating the direction of the lattice distortion (Fig. 7). The refinement of the occupancy for this atom confirmed a significant deviation from full occupancy; no occupancy deviations were observed for Pr ands Se(1). The composition was computed to $PrSe_{1.85(1)}$.

First- and second-order harmonics for the occupancy modulation of Se(2) were then introduced to start the refinement of the modulated structure. From the calculated Fourier maps around Se(2), cf. Fig. 8, e.g., it is apparent, that the atom Se(2) partly follows a saw tooth-like modulation. Such a discontinuous behavior is quite well known for site occupancy modulations, but unfortunately a step-like function is not available for (3+2)-dimensional problems in the refinement software. Harmonic functions with coefficients up to the order of 3 along each modulation wave for occupational and positional modulation of Se(2) have been chosen as approximation instead. The harmonic function is developed into a truncated

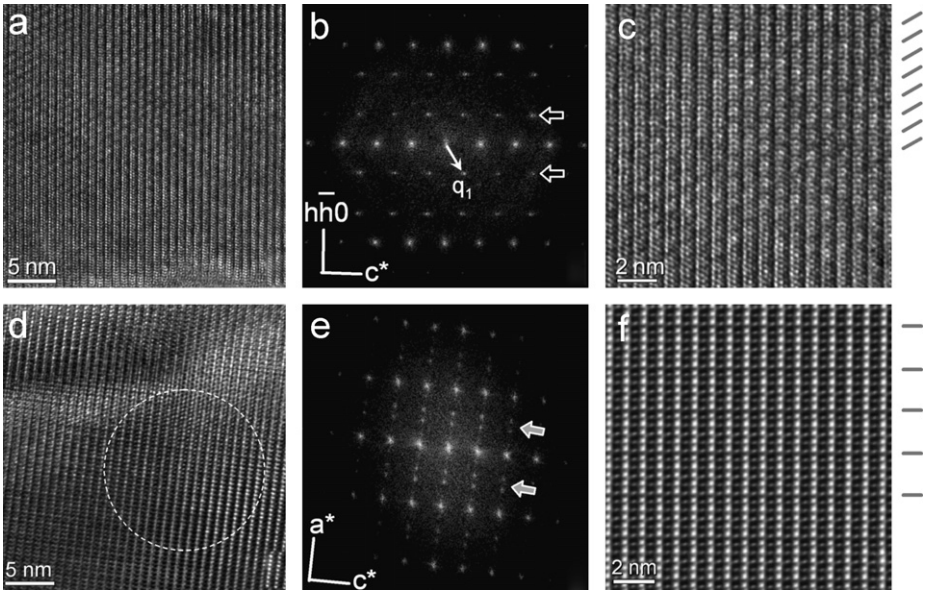


Fig. 6. (a) High-resolution TEM image of a $PrSe_{1.85}$ crystal along [$\bar{7}$ 7 4]; (b) Corresponding Fourier Transform showing the satellite reflections around each main reflection; two black arrows indicate lines of satellites, the modulation vector $q_1$ is indicated; (c) enlarged section of the TEM image a, the modulation period is indicated by the gray lines on the right; (d) HRTEM image of a $PrSe_{1.85}$ crystal along the [0 1 0] direction; (e) Fourier Transform of 6d, double lines of satellites attributed to the modulation vectors $\pm(q_1+q_2)$ and $\pm(q_1-q_2)$ are indicated by gray arrows; (f) filtered, averaged and enlarged image of region enclosed by a white circle in TEM image 6d, the modulation period is indicated by the grey lines on the right.

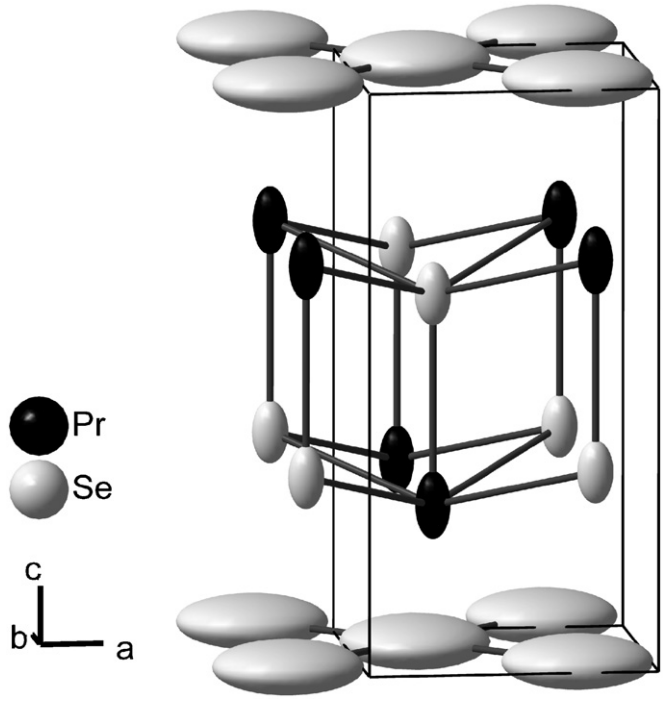


Fig. 7. Average structure of $PrSe_{1.85}$, thermal ellipsoids at a 99.9 probability level, the unit cell is indicated, [22].

Fourier series and the Fourier coefficients are treated as refineable parameters during the calculations. The positional modulations of Pr and Se(1) atoms were fitted harmonically, too, with first and second order Fourier coefficients for the respective modulation waves. As can be extracted from the Fourier sections in Fig. 9, e.g., calculated positions and electron density distributions match quite well for these atoms. In the final stages of the refinement, harmonic modulation waves for the displacement parameters of all atoms were introduced. The structure model then converged to final residuals of $R_1 = 0.094$ and $wR_2 = 0.148$ for all 2680 independent reflection (main reflections, first and second order satellites, higher-order satellites were excluded from the refinement due to their very low intensities), the occupancy modulation of Se(2) gave the composition $PrSe_{1.854(7)}$. The resulting crystallographic parameters are given in Tables 4–6, interatomic distances can be found in Table 7. Further details of the crystal structure investigation may be obtained from Fachinformationszentrum Karlsruhe, D–76344 Eggenstein-Leopoldshafen, Germany (fax: (+49)7247-808-666; e-mail: crysdata@fiz-karlsruhe.de) on quoting the deposition number CSD-416866.

The crystal structure of $PrSe_{1.85}$ can be described as a stacking sequence of puckered [PrSe(1)] double sheets and planar [Se(2)] layers, cf. image of the average crystal structure in Fig. 7. The same basic structure is found for all rare earth polychalcogenides $LnX_{2-\delta}$ ($Ln$ = Y, La, Ce–Lu; $X$ = S, Se, Te; $0 \leqslant \delta \leqslant 0.3$) of trivalent metals ($Ln^{3+}$). Disregarding distortion and vacancies in the planar Se(2) layers, this structural pattern can be attributed to the ZrSSi structure type [14]. As can be extracted from the Fourier maps (Figs. 8 and 9), the modulation mainly affects the Se(2) atoms of the planar layer. The Se(2)-layer of $PrSe_{1.85}$ contains 15% vacancies compared to the stoichiometric diselenide $PrSe_2$. By introducing these vacancies, the

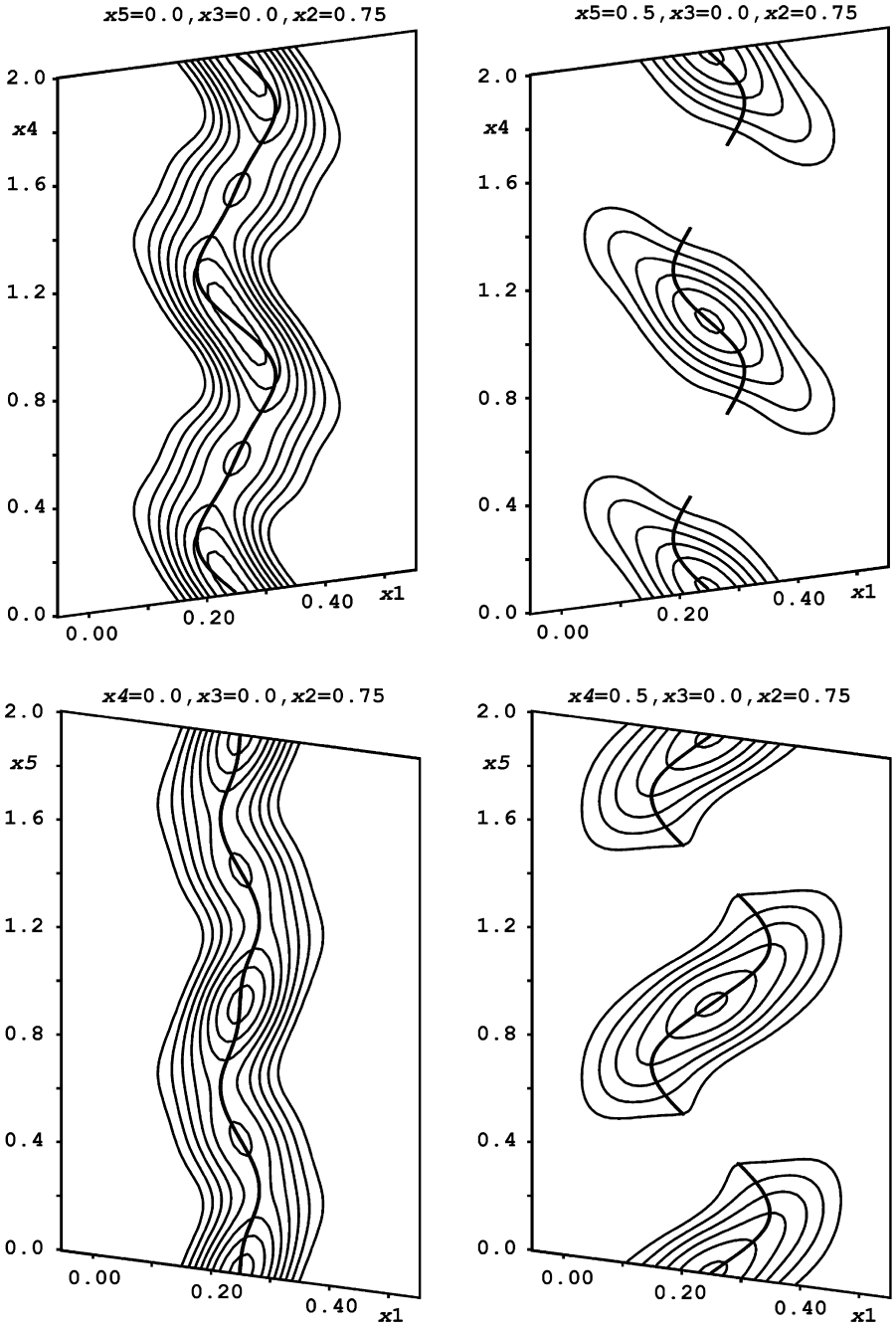


Fig. 8. Fourier sections around Se(2), the electron density is displayed in steps of 20 e $Å^{-3}$, the thick central lines denote the calculated atomic position.

remaining Se atoms of the layer are forced to re-arrange with respect to both, the idealized non-modulated structure containing an undistorted planar square layer [14] and the commensurately modulated $PrSe_2$ containing a herring-bone pattern of $Se_2^{2-}$ dimers [4].

Different Fourier sections calculated around Se(2) confirm, that the major part of the positional modulation of this atom is found in the crystallographic $a$ and $b$ directions, whereas the displacement along $c$ is much smaller. Fig. 8 gives the Fourier sections $x4$–$x1$ for $x5 = 0$ and 0.5 and $x5$–$x1$ for $x4 = 0$ and 0.5 as examples ($x1$, $x2$ and $x3$ correspond to the crystallographic directions $a$, $b$ and $c$, $x4$ and $x5$ correspond to the directions of the modulation vectors $q_1$ and $q_2$, respectively). As can be seen from the electron density distribution at different regions in superspace, the atomic rod is separated in discrete regions along $x4$. For the regions $x4 = 0.6$ and $x5 = 0.5$, as well as for $x5 = 0.4$ and $x4 = 0.5$ (right hand side of Fig. 8) the electron density is close to zero. This is mirrored by the calculated atomic position, the atomic line function is interrupted here.

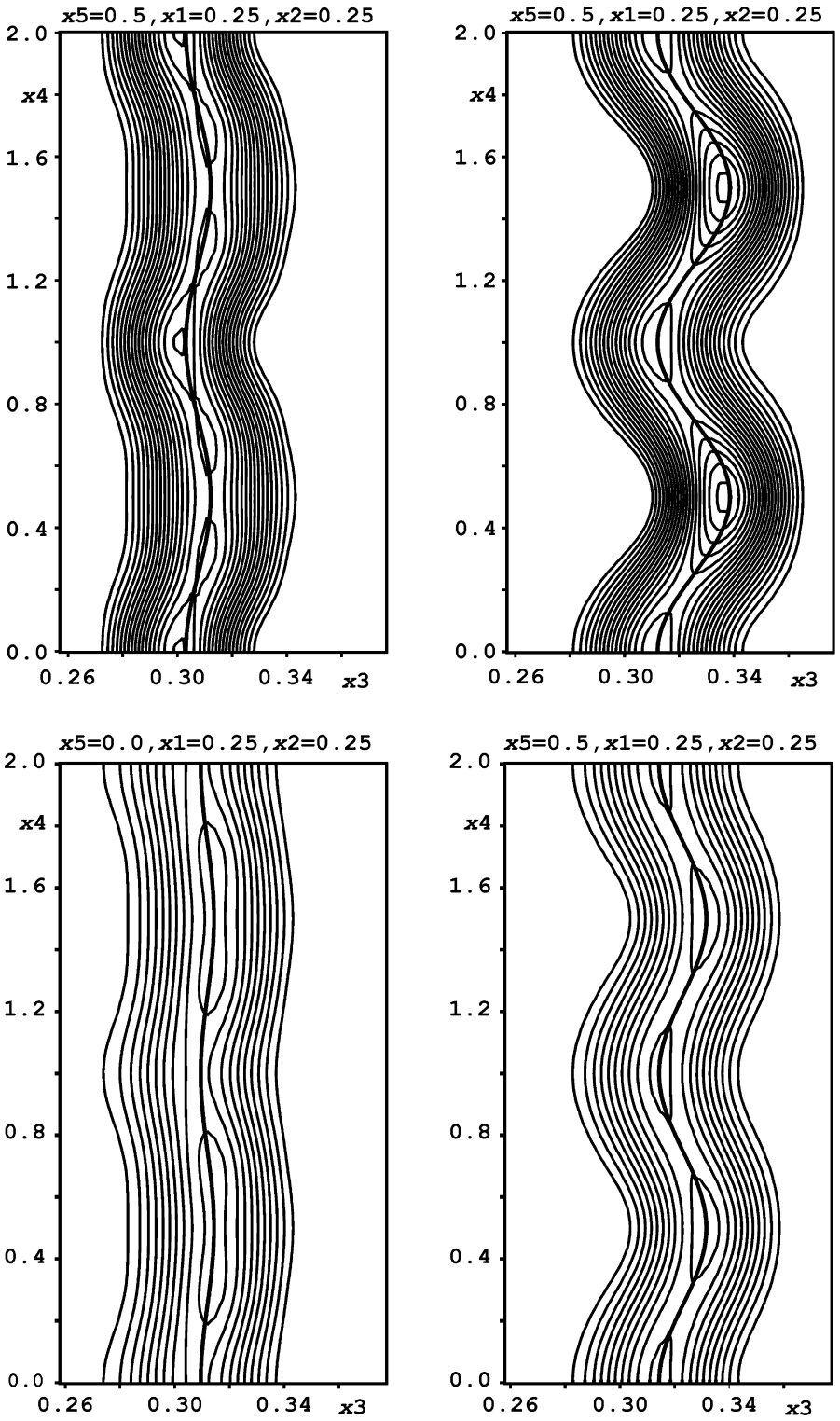


Fig. 9. Fourier sections around Pr (top) and Se(1) (bottom), the electron density is displayed in steps of 20 e Å$^{-3}$, the thick central lines denote the calculated atomic position.

The modulational displacements for Pr and Se(1) are much greater along the crystallographic $c$ direction than along $a$ or $b$ and the amount of displacement is greater for praseodymium. This can be understood as a direct reaction to the strong modulation in the Se(2) layer which affects the coordination sphere of the Pr atoms most. The Se(1) atoms on the other hand have to react to the shift of the Pr atoms only. Fig. 9 shows two Fourier sections $x4$–$x3$ for $x5 = 0$ and 0.5 calculated around Pr and Se(1) to visualize the displacements of both atoms.

Table 4
Crystallographic and refinement data for $PrSe_{1.85}$

| | |
|---|---|
| Formula; formula weight; $F(0\,0\,0)$ | $PrSe_{1.85(1)}$; 278 g mol$^{-1}$; 488 |
| Crystal size | $0.01 \times 0.04 \times 0.06$ mm$^3$ |
| Diffractometer, radiation | STOE IPDS-2, graphite monochromator, Mo$K\alpha$ |
| Meas. Temperature | 120 K |
| Reflections | $-6 \leqslant h,k \leqslant 6$; $-20 \leqslant l \leqslant 24$; $-2 \leqslant m,n \leqslant 2$<br>$2.0 \leqslant \theta \leqslant 30.6^\circ$; 54,255 reflections collected |
| Main reflections and satellites | 2860 independent, 1652 obs. with $I > 3\sigma(I)$ |
| Main reflections only | 226 independent, 222 obs. with $I > 3\sigma(I)$ |
| First order satellites | 884 independent, 651 obs. with $I > 3\sigma(I)$ |
| Second order satellites | 1750 independent, 779 obs. with $I > 3\sigma(I)$ |
| $R_{int}$; $R_{sigma}$ | 0.215; 0.051 |
| Superspace group; $Z$ | $P4/n(\alpha\beta\frac{1}{2})(\beta-\alpha\frac{1}{2})00$ (No. 2539; [13]); 4 |
| Centering vector | (0, 0, $\frac{1}{2}$, $\frac{1}{2}$, $\frac{1}{2}$) |
| Lattice parameters | $A = 4.147(1)$ Å<br>$C = 16.838(2)$ Å<br>$V = 289.3(1)$ Å$^3$ |
| Modulation vectors | $q'_1 = (-0.293(1), 0.293(1), 0)$,<br>$q'_2 = (0.293(1), 0.293(1), 0)$ |
| Calc. density; abs. coefficient | 6.59 g cm$^{-3}$; 39.8 mm$^{-1}$ |
| Abs. correction | Analytical [7], $T_{min} = 0.06$, $T_{max} = 0.21$ |
| Modulation functions | Harmonic for occupation of Se(2), site parameters and *adp*'s of Pr and Se(1)[a] |
| Modulation waves | $1 \cdot q'_1$, $1 \cdot q'_2$, $(q'_1 + q'_2)$, $(q'_1 - q'_2)$, $2 \cdot q'_1$, $2 \cdot q'_2$ |
| Refinement | JANA2000, full matrix against $F^2$ [7]<br>72 parameters, no restraints |
| Weighting scheme | $w = 1/[\sigma^2(I) + 0.0036(I^2)]$ |
| Agreement factors | $R_1$, w$R_2(I > 3\sigma)$; $R_1$, $wR_2$(all $I$) |
| Overall | 0.050, 0.127; 0.094, 0.148 |
| Main reflections | 0.027, 0.072; 0.027, 0.072 |
| First order satellites | 0.038, 0.089; 0.059, 0.100 |
| Second order satellites | 0.106, 0.216; 0.205, 0.256 |
| GooF (all $I$) | 1.24 |
| Largest diff. peak/hole | $+5.60/-5.52$ e Å$^{-3}$ |

[a] *adp*: anisotropic displacement parameters.

Table 5
Atomic coordinates, occupancies and coefficients $U_{ij}$ of the tensors of the anisotropic displacement parameter/Å$^2$ for $PrSe_{1.85}$

| Atom | occ. | $x$ | $y$ | $Z$ | $U_{11} = U_{22}$ | $U_{33}$ |
|---|---|---|---|---|---|---|
| Pr | 1 | $\frac{1}{4}$ | $\frac{1}{4}$ | 0.13668(2) | 0.0066(2) | 0.0092(3) |
| Se(1) | 1 | $\frac{1}{4}$ | $\frac{1}{4}$ | 0.31773(4) | 0.0067(3) | 0.0079(3) |
| Se(2) | 0.854(7) | $\frac{1}{4}$ | $\frac{3}{4}$ | 0 | 0.0170(7) | 0.0067(7) |

The change of the occupancy of the atoms Se(2) along $t$ ($t$ is the internal coordinate associated with $q_1$) is displayed in the top of Fig. 10 for two different values of $u$ (the respective internal coordinate associated with $q_2$). The shape of the occupation function clearly resembles the harmonic approximation of the structure model. For $u = 0$, the minimum occupancy is about 0.45, for $u = 0.2$ the curve drops to approximately zero.

The variation of the Se(2)–Se(2) distances along $t$ is depicted in the bottom of Fig. 10, again for $u = 0$ and 0.2. The non-modulated distances in the average structure are given as dashed lines. As can be seen, the variation of two Se–Se distances in the layer is quite large (2.35–3.50 Å) along $t$, the variation of the two others is smooth (2.25–2.50 Å and 3.20–3.40 Å). One distance is in general much shorter than the others, indicating bonding interaction between two adjacent Se atoms and the formation of a $Se_2^{2-}$ dimer over the complete modulation period. The longest distance with an average value of 3.3 Å must be regarded as non-bonding over the whole modulation period, whereas the two others change between bonding and non-bonding. In both $t$-plots, at $u = 0.2$, two of the curves are interrupted due to the missing of the respective Se atoms. In order to compensate for the loss of one atom, the remaining Se–Se distances then adopt the shortest values observed in the structure. The interruption corresponds directly to the occupancy curve above. The $t$-plots for the respective Pr–Se-distances are not displayed here.

The modulated Se(2) layer is depicted in Fig. 11. Only positions with occupancy greater than 0.45 are shown as

Table 6
Non-zero Fourier coefficients $S$ (sine) and $C$ (cosine) of the harmonic modulation function[a] of the site modulation waves ($x$, $y$, $z$) and the occupancy modulation waves (*occ*) for $PrSe_{1.85}$; subscripts 1 and 2 refer to the modulation waves $1\cdot q'_1$ and $1\cdot q'_2$, 3 and 4 to $(q'_1+q'_2)$ and $(q'_1-q'_2)$, and 5 and 6 to $2\cdot q'_1$ and $2\cdot q'_2$, resp.

| | Pr | Se(1) | Se(2) |
|---|---|---|---|
| $S_{x1}=-S_{y2}$ | −0.0045(2) | 0.0016(3) | −0.0580(7) |
| $S_{y1}=S_{x2}$ | −0.0064(2) | −0.0028(3) | 0.0612(5) |
| $C_{z1}=C_{z2}$ | 0.00891(3) | −0.00560(4) | 0.0008(1) |
| $S_{x3}=-S_{y4}$ | 0.0012(3) | −0.0010(5) | −0.0180(8) |
| $S_{y3}=S_{x4}$ | 0.0039(1) | −0.0009(1) | −0.0163(4) |
| $C_{z3}=C_{z4}$ | 0.00219(3) | 0.00157(4) | −0.00059(5) |
| $S_{x5}=-S_{y6}$ | — | — | −0.0149(7) |
| $S_{y5}=S_{x6}$ | — | — | −0.0130(7) |
| $C_{z5}=-C_{z6}$ | — | — | −0.0031(1) |
| $C_{o1}=C_{o2}$ | — | — | 0.234(5) |
| $C_{o3}=C_{o4}$ | — | — | −0.151(6) |
| $C_{o5}=C_{o6}$ | — | — | −0.062(6) |

[a]The general positional atomic modulation function $M$ is given as a sum of harmonic functions, $M_x(v)$ can be expressed as $M_x(v)=\sum_{n=1}^{m} S_{xn}\sin(2\pi nv)+C_{xn}\cos(2\pi nv)$.Similar expressions are obtained for $M_y(v)$and $M_z(v)$ and for the occupancy $M\mathrm{occ}(v)$, respectively.

Table 7
Selected interatomic distances/Å for $PrSe_{1.85}$

| Atoms | Ave. | Min. | Max. | $\Delta_{max.-min.}$ |
|---|---|---|---|---|
| Pr–Se(1) | 3.053(2) | 2.916(3) | 3.139(3) | 0.223 |
| | 3.035(3) | 2.952(4) | 3.100(3) | 0.184 |
| | 2 × 3.036(3) | 2.952(4) | 3.100(3) | 0.184 |
| | 3.037(3) | 2.952(4) | 3.100(3) | 0.184 |
| Pr–Se(2) | 3.112(7) | 2.906(8) | 3.349(8) | 0.443 |
| | 3.120(7) | 2.907(8) | 3.349(8) | 0.442 |
| | 3.122(7) | 2.907(8) | 3.349(8) | 0.442 |
| | 3.126(7) | 2.906(8) | 3.348(8) | 0.442 |
| Se(2)–Se(2) | 2.918(11) | 2.266(10) | 3.652(10) | 1.386 |
| | 2.934(11) | 2.264(10) | 3.654(10) | 1.390 |
| | 2.960(11) | 2.264(10) | 3.654(10) | 1.390 |
| | 2.971(11) | 2.264(11) | 3.654(10) | 1.390 |

occupied, this represents the composition of the compound as [PrSe(1)] $[Se(2)]_{0.85}$ best. As could be expected from the distance-*t*-plots for Se(2), the distribution of Se–Se-distances gives no clear indication of nearest neighbors and shows no apparent separation between short (bonding) and longer (non-bonding) distances. However, Se–Se distances between 2.25 and 2.56 Å are indicated as thick lines, distances between 2.60 and 2.89 Å as dotted lines, in Fig. 11. If only the shorter distances are taken into account, the layer should be described as consisting of vacancies, isolated $Se^{2-}$ anions, $Se_2^{2-}$ dimers and bent $Se_3$ fragments. The latter could be regarded as trimeric $Se_3^{2-}$ anions, they could as well consist of a disordered pair of one $Se_2^{2-}$ dimer and one $Se^{2-}$. It is not possible to distinguish between these two cases based on the present data. The bond angle within the trimeric units is in the range of 90°. This is considerably smaller than the bond angle in the well-known bent triselenide anions (approximately 110°) found in alkali metal triselenides $A_2Se_3$ ($A$ = Na, K, Rb, Cs; e.g., [15]). However the trimers in the alkali metal compounds are well separated from each other and this is definitely not the case for $PrSe_{1.85}$. In the present structure we find distances well below 3 Å between several anionic fragments, which is much smaller than the van-der-Waals distance between two selenium atoms of 3.80 Å, [16]. A stabilizing interaction between the selenium entities must be taken into account.

If distances up to 2.89 Å are considered, linear triatomic anions and fragments of eight-membered rings appear in the structure image. The triatomic entities can either be considered as $XeF_2$-like $Se_3^{4-}$ or as a disordered pattern of two dimers. Again, a definite resolution of this question is not possible from our data. The fragments of the eight-membered rings are found surrounding single vacancies. The same arrangement is also found in the related, but commensurately modulated, compounds of the $CeSe_{1.9}$ type [17] and in $Gd_8Se_{15}$ ($GdSe_{1.875}$, [18]). Another feature in the modulated Se layer of $PrSe_{1.85}$ is the occurrence of two adjacent vacancies caused by the missing of $Se_2^{2-}$ dimers. This characteristic has only been found in rare earth polychalcogenides $LnX_{2-\delta}$ with $\delta \geqslant 0.15$ so far, compounds with higher selenium content do not show these double vacancies.

The modulation of $PrSe_{1.85}$ resembles striking similarities to the modulated structure of $Nd_{0.6}Gd_{0.4}Se_{1.85}$ [19b]. The lattice parameters and modulation vectors of both compounds are comparable. Their diffraction images are both compatible with tetragonal symmetry and their structures were refined in the same tetragonal superspace group yielding modulated Se layers which are very much alike. Based on the same average structure, the two-dimensionally modulated structure of $DySe_{1.84}$ [19a] is compatible with orthorhombic symmetry at most (lattice parameters $a = 3.991$ Å, $b = 3.986$ Å and $c = 8.206$ Å, modulation vectors $q_1 = (\alpha, \beta, \frac{1}{2})$ and $q_2 = (\alpha, -\beta, \frac{1}{2})$ with $\alpha = 0.333$ and $\beta = 0.273$). The vacancies in the modulated Se layer of the latter compound are the result of missing Se-dimers only.

## 4. Conclusions and outlook

Tensimetric studies have shown, that the Pr–Se phase diagram contains the discrete polyselenides $PrSe_{2-x}$ with $x = 0$, 0.1, 0.15 and 0.2. The fractional compositions of these compounds can be converted to the rational formulae $Pr_{10}Se_{19}$ ($PrSe_{1.90}$), $Pr_7Se_{13}$ ($PrSe_{1.85}$), $Pr_5Se_9$ ($PrSe_{1.80}$) and attributed to a homologous series of the generic formula $Pr_nSe_{2n-1}$ with $n = 10$, 7, and 5, respectively. These compounds must be regarded as phases without homogeneity range, i.e., "line compounds". Selenium-richer polyselenides $PrSe_n$ with $n > 2$ (e.g., $PrSe_{2.33}$) could not be prepared under the synthetic conditions used.

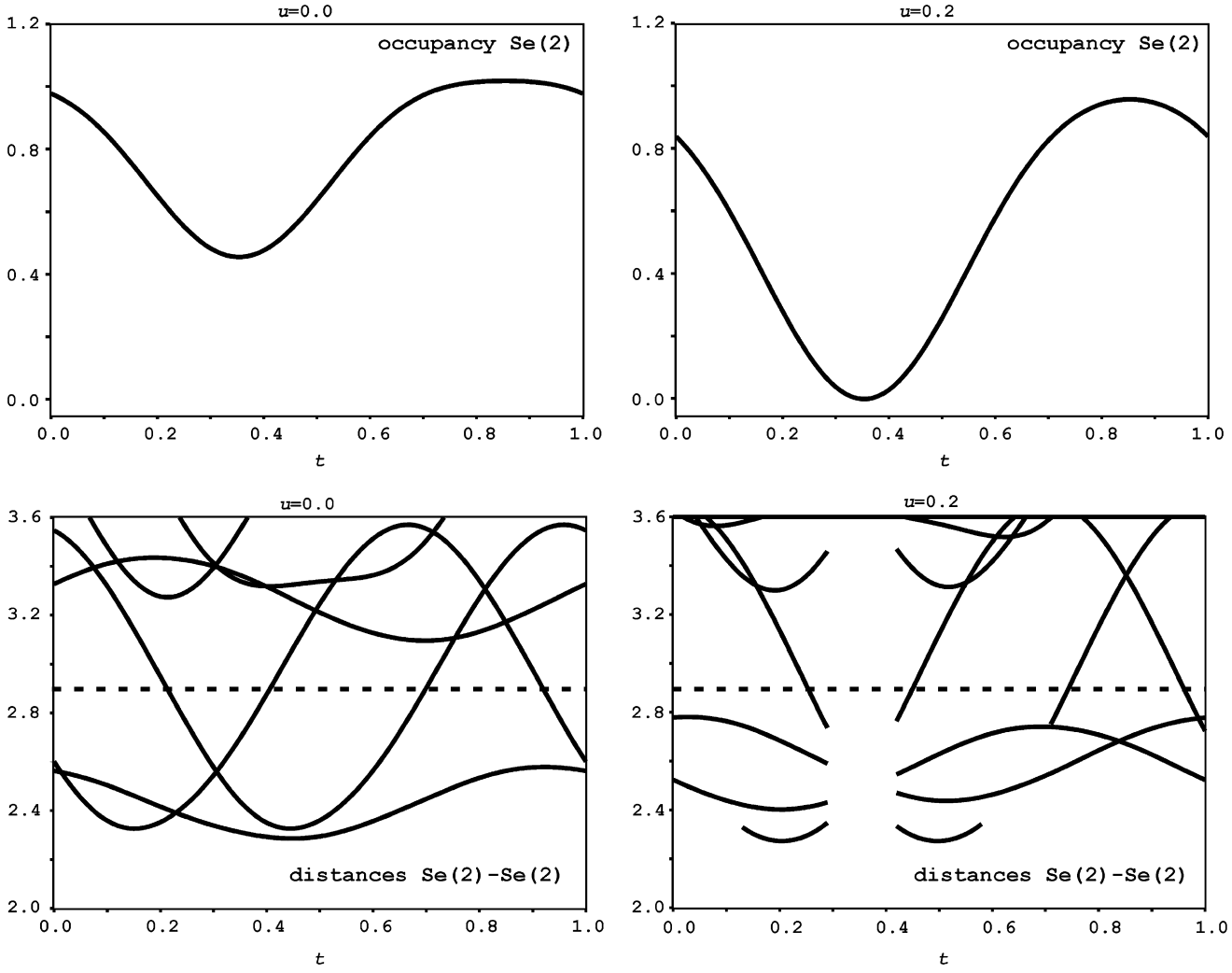


Fig. 10. top: Occupancy-$t$-plots for Se(2) for $u = 0$ and 0.5; bottom: distance-$t$-plots for Se(2)–Se(2) distances.

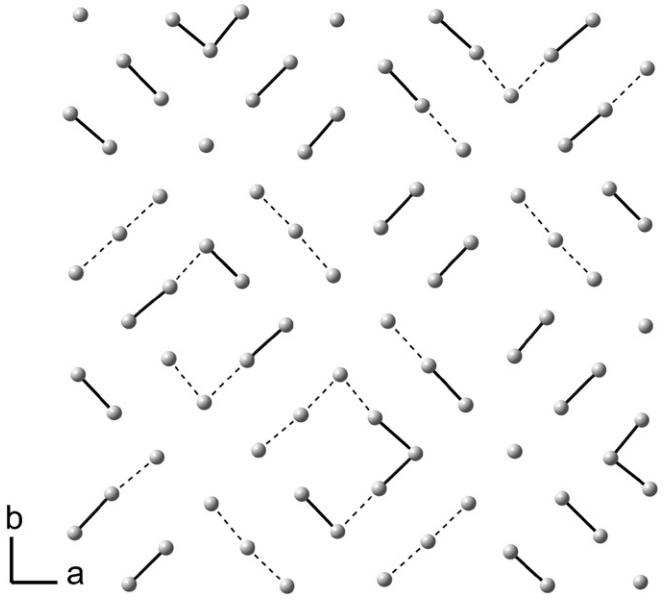


Fig. 11. Section of the modulated Se layer of $PrSe_{1.85}$ Se–Se-distances between 2.25 and 2.56 Å are indicated as thick lines, distances between 2.60 and 2.89 Å as dotted lines, [22].

The existence of the new phase $PrSe_{1.85}$ is confirmed by thermogravimetry, TEM investigations and X-ray structure analysis. The structure of $PrSe_{1.85}$, like that of all other polyselenides of trivalent rare earth metals, can be understood as superstructure of the basic ZrSSi type. A structure model of incommensurately modulated $PrSe_{1.85}$ could be evolved in superspace group $P4/n(\alpha\beta\frac{1}{2})(\beta\text{–}\alpha\frac{1}{2})00$. The origin of the two-dimensional modulation is a site occupancy wave and, coupled to this, a charge density wave in the planar selenium layer. The modulated Se(2) layers mainly consist of $Se_2^{2-}$ dimers, $Se^{2-}$ anions and vacancies and resemble some similarities to the respective layers of the incommensurate structures of $Nd_{0.6}Gd_{0.4}Se_{1.85}$ and $DySe_{1.84}$ as well as to the commensurate superstructures of the $CeSe_{1.9}$ type and of $GdSe_{1.875}$. The main difference between the commensurate and incommensurate rare earth polyselenides lies in the lower selenium content which enforces adjacent vacancies in the modulated Se layers. The synthesis and structure solution of the selenium-poor polychalcogenides $PrSe_{2-x}$ with $x > 0.15$ identified in this work remains a challenging task for the future. Further tensimetric and structural investigations will also expand

on other rare earth–chalcogen systems in order to gain detailed insight into different types of defects and defect structures of rare earth polychalcogenides.

## Acknowledgments

The authors thank Prof. Dr. H. Lichte, Institute of Structure Physics (ISP), Dresden University of Technology, for supporting the TEM investigations, Dr. W. Schnelle, Max Planck Institute for Chemical Physics of Solids, Dresden, for the magnetic measurements, Drs. T. Chusova and L. Zelenina, both A. V. Nikolaev Institute of Inorganic Chemistry, Russian Academy of Sciences, Novosibirsk, for tensimetric measurements and Mrs. E. Kern, Dresden University of Technology, for performing the EDX analyses. Financial support by the Deutsche Forschungsgemeinschaft is gratefully acknowledged.

## References

[1] (a) P. Vilars (Ed. in Chief): Pauling File Binaries Edition, JST, Tokyo, Japan & MDPS, Vitznau, Switzerland, 2001;
(b) T.B. Massalski (Ed.), Binary Alloy Phase Diagrams, ASM, Materials Par (OH), USA, 1990.
[2] P. Plambeck-Fischer, W. Abriel, W. Urland, J. Solid State Chem. 78 (1989) 164.
[3] (a) E.I. Yarembash, A.A. Eliseev, V.I. Kalitin, L.I. Antonova, Izv. Akad. Nauk SSSR, Neorg. Mater. 2 (1966) 984;
(b) V.I. Kalitin, E.I. Yarembash, N.P. Luzhnya, Izv. Akad. Nauk SSSR, Neorg. Mater. 2 (1966) 1672;
(c) E.I. Yarembash, A.A. Eliseev, in: Rare Earth Chalcogenides. Synthesis and Crystal Chemistry; Nauka, Moscow, USSR, 1975, p. 258;
(d) A.A. Eliseev, A.A. Grizik, Defect formation in rare earth element chalcogenides, in: V.P. Zhuze, I.A. Smirnov (Eds.), Redkozemelnie Poluprovodniki, Nauka, Leningrad, USSR, 1977, p. 146.
[4] Th. Doert, C. Graf, Z. Allg. Anorg. Chem. 631 (2005) 1101.
[5] (a) V.B. Lazarev, J.H. Greenberg, B.A. Popovkin, In: E. Kaldis (Ed.), Current Topics in Materials Science, North-Holland, Amsterdam, 1978, p. 657–695;
(b) I.G. Vasilyeva, E.I. Beljaeva, J. Solid State Chem. 142 (1999) 261.
[6] X-AREA, IPDS Software, STOE & Cie., Darmstadt, 2006.
[7] V. Petricek, M. Dusek, JANA2000, Crystallographic Computing System, Prague, 2006.
[8] P.J. Becker, P. Coppens, Acta Crystallogr. A 30 (1974) 129;
P.J. Becker, P. Coppens, Acta Crystallogr. A 30 (1974) 148.
[9] M. Folchnandt, Th. Schleid, Z. Anorg. Allg. Chem. 627 (2001) 1411.
[10] (a) J. Berkowitz, W. Chupka, J. Chem. Phys. 45 (1966) 4289;
(b) J. Berkowitz, W. Chupka, J. Chem. Phys. 48 (1968) 5743.
[11] G. Krabbes, W. Bieger, K.-H. Sommer, T. Söhnel, GMIN (Vers. 4.01), part of the Program Package TRAGMIN for Calculation of Equilibria, Dresden, 1995.
[12] A. Weiss, H. Witte, Magnetochemie, Verlag Chemie, Weinheim, 1973.
[13] A. Yamamoto, Acta Crystallogr. A 52 (1996) 509.
[14] A.J. Klein Haneveld, F. Jellinek, J. Less-Common Metal 24 (1971) 229.
[15] (a) P. Böttcher, Z. Anorg. Allg. Chem. 432 (1977) 167;
(b) P. Böttcher, Z. Anorg. Allg. Chem. 461 (1980) 13.
[16] A. Bondi, J. Phys. Chem. 68 (1964) 441.
[17] (a) P. Plambeck-Fischer, W. Abriel, W. Urland, J. Solid State Chem. 78 (1989) 164;
(b) W. Urland, P. Plambeck-Fischer, M. Grupe, Z. Naturforsch. B 44 (1989) 261;
(c) M. Grupe, W. Urland, J. Less-Common Metal 170 (1991) 271;
(d) E. Dashjav, Th. Doert, P. Böttcher, Hj. Mattausch, O. Oeckler, Z. Kristallogr. NCS 215 (2000) 337.
[18] (a) K.G. Adams, Diploma Thesis, Karlsruhe, 1993;
(b) Th. Doert, E. Dashjav, B.P.T. Fokwa, Z. Anorg. Allg. Chem., in press.
[19] (a) A. van der Lee, L.M. Hoistad, M. Evain, B.J. Foran, S. Lee, Chem. Mater. 9 (1997) 218;
(b) Th. Doert, B.P.T. Fokwa, S. Lidin, F.J.G. García, J. Solid State Chem. 177 (2004) 1598.
[20] O. Knacke, O. Kubaschewski, K. Hesselmann, Thermochemical Properties of Inorganic Substances, Second Ed, Springer, New York, 1991.
[21] (a) K.C. Mills, Thermodynamic Data for Inorganic Sulphides, Selenides and Tellurides, London Butterworths, Redwood Press limited, Trowbridge, Wiltshire, 1974;
(b) M. Binnewies, E. Mielke, Thermochemical Data of Elements and Compounds, Viley-VCH, Weinheim, 1999.
[22] DIAMOND, Crystal Impact GbR, Bonn, Germany, 2006.